

Ultrafast magnetization dynamics in pure and doped Heusler and inverse Heusler alloys

R. Chimata,^{1,2} E. K. Delczeg-Czirjak,² J. Chico,³ M. Pereiro,² B. Sanyal,² O. Eriksson,^{2,4} and D. Thonig²

¹Argonne National Laboratory, Lemont, IL 60439, United States

²Department of Physics and Astronomy, Materials Theory, University Uppsala, SE-75120 Uppsala, Sweden

³Peter Grünberg Institut and Institute for Advanced Simulation,

Forschungszentrum Jülich & JARA, D-52425 Jülich, Germany

⁴School of Science and Technology, Örebro University, SE-701 82 Örebro, Sweden

(Dated: February 2, 2022)

By using a multiscale approach based on first-principles density functional theory combined with atomistic spin dynamics, we investigate the electronic structure and magnetization dynamics of an inverse Heusler and a Heusler compound and their alloys, i. e. $\text{Mn}_{2-x}\text{Z}_x\text{CoAl}$ and $\text{Mn}_{2-x}\text{Z}_x\text{VAl}$, where $\text{Z} = \text{Mo}, \text{W}, \text{Os}$ and Ru , respectively. A signature of the ferrimagnetic ordering of Mn_2CoAl and Mn_2VAl Heusler alloys is reflected in the calculated Heisenberg exchange constants. They decay very rapidly with the interatomic distance and have short range, which is a consequence of the existence of the finite gap in the minority spin band. The calculated Gilbert damping parameter of both Mn_2CoAl and Mn_2VAl is high compared to other half-metals, but interestingly in the particular case of the inverse Mn_2CoAl alloys and due to the spin-gapless semiconducting property, the damping parameters decrease with the doping concentration in clear contradiction to the general trend. Atomistic spin dynamics simulations predict ultrafast magnetisation switching in Mn_2CoAl and Mn_2VAl under the influence of an external magnetic field, starting from a threshold field of 2 T. Our overall finding extends with Heusler and inverse Heusler alloys, the class of materials that exhibits laser induced magnetic switching.

I. INTRODUCTION

The field of the ultrafast magnetization dynamics has become one of the most important topics in magnetism, starting from the pioneering experiment on ferromagnetic nickel from Beaupaire et al.¹ in 1996. Since then, numerous experiments were carried out on 3d (Fe^2 , Co^3 , $\text{Ni}^{4,5}$), 4f (Tb and Gd⁶) ferromagnets, as well as on several alloys (GdFeCo^{7-13} , TbCo^{14} , CoPt^{15}) and half metallic systems (CrO_2^{16} , $\text{Co}_2\text{Cr}_{0.6}\text{Fe}_{0.4}\text{Al}^{17}$, Co_2FeSi , Co_2MnGe , $\text{Co}_2\text{FeAl}^{18}$, and $\text{Co}_2\text{Fe}_x\text{Mn}_{1-x}\text{Si}^{19}$ and $\text{Co}_2\text{MnSi}^{19,20}$) aiming to find faster ways of manipulating spins in a controllable way, opening a new field in the advanced information/data storage and data processing technologies.

Experimental observations revealed that the characteristic demagnetization times of 3d elements are within the 100 fs time scale, much faster than that of the 4f-ferromagnets, which show more complex behavior involving a two-step demagnetization process in 10 ps time scale. Surprisingly, recent pump-probe experiments on half-metallic Heusler alloys measured distinguished and typically larger all-optical switching times when compared to 3d-ferromagnets^{8,19}. In these materials, one of the spin channels is completely or partially unoccupied around the Fermi energy, consecutively the magneto optical excitations from one channel to another channel are forbidden.

Attempts to understand the momentum transfer between the electrons, spins and phonons after a short laser pulse have opened a new debate in the field. Several quantitative models had been proposed to describe the mechanism of the ultrafast demagnetization such

as the microscopic three-temperature model²¹, stochastic atomistic descriptions²², models using the stochastic Landau-Lifshitz-Bloch equation^{23,24} and models suggesting the presence of diffusive or superdiffusive spin currents^{6,25-28}. The first three models relate the spin-scattering to the Gilbert damping parameter, α , that describes the energy dissipation in a magnetic system via elementary spin-flip processes^{29,30}. Here, we combine the *ab initio* description of the magnetic exchange interaction and Gilbert damping³¹⁻³³ parameter with the Landau-Lifshitz-Gilbert equation to investigate the demagnetization process in half-metallic ferrimagnetic Heusler and inverse Heusler alloys.

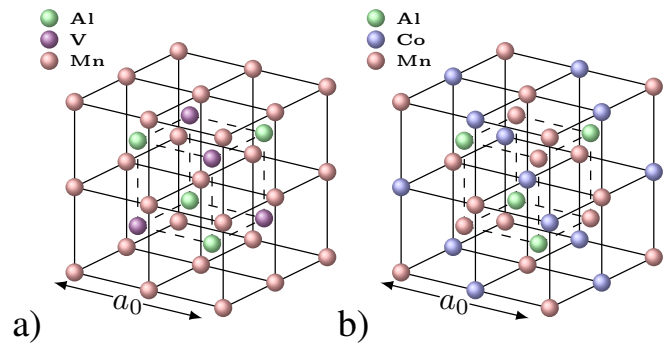


FIG. 1. (Color online) Schematic crystal structures of a) the Heusler alloy Mn_2VAl and b) the inverse Heusler alloy Mn_2CoAl . Different atom types are represented by different colours. Solid and dashed lines indicate the bond between the atoms and are added to guide the eye. The lattice constant a_0 is also indicated.

Heusler and inverse Heusler alloys are defined as ternary intermetallic compounds with a composition of X_2YT (cf. Fig. 1). Heusler alloys crystallize in the $L2_1$ structure (space group $Fm\bar{3}m$, 225), with the $4a$ (0, 0, 0), $4b$ ($\frac{1}{2}, \frac{1}{2}, \frac{1}{2}$) and $8c$ ($\frac{1}{4}, \frac{1}{4}, \frac{1}{4}$) Wyckoff positions. X and Y are transition metals occupying the $8c$ and $4a$ positions, respectively, and T is a main group III, IV or V element sitting in the $4b$ position. Inverse Heusler alloys adopt the Hg_2CuTi prototype structure (space group $F\bar{4}3m$, 216), with $4a$ (0,0,0), $4b$ ($\frac{1}{2}, \frac{1}{2}, \frac{1}{2}$), $4c$ ($\frac{1}{4}, \frac{1}{4}, \frac{1}{4}$) and $4d$ ($\frac{3}{4}, \frac{3}{4}, \frac{3}{4}$) positions. In this case, X and Y are transition metals, X occupying the $4a$ and $4d$ positions while Y is the $4c$ position. The main element T sits in the $4b$ position. Both structures may be regarded as a cubic unit cell, which consists of four interpenetrating fcc sublattices. There are four atoms in the diagonal of the cube following the X - Y - X - T sequence for Heusler alloys and X - X - Y - T for the inverse Heuslers.

Here, we study the demagnetization dynamics of a Heusler and an inverse Heusler compound and their alloys, i.e. $Mn_{2-x}Z_xVAl$ and $Mn_{2-x}Z_xCoAl$, where $Z = Mo, W, Os$ and Ru . Mn_2VAl is a well known half-metallic ferrimagnetic Heusler compound^{34–39} where the minority spin channel is the conducting one⁴⁰. Mn_2CoAl adopts the inverse Heusler structure⁴¹ and it is predicted⁴¹ and confirmed⁴² to be a spin gapless magnetic semiconductor. These peculiarities of the band structure are reflected in the Gilbert damping parameter and affect the magnetisation dynamics under the influence of a laser pulse, as will be described below.

The paper is divided as follows: In Section II we introduce our numerical technique to study materials properties and magnetization dynamics in Heusler alloys. Electronic and magnetic properties of the parent Heusler alloys Mn_2CoAl and Mn_2VAl as well as doping of these materials with Os, Ru, W , and Mo is discussed in Section III A. Demagnetisation studies of these alloys caused by a femtosecond laser are described in Section III E. Finally, the article concludes in Section IV with an outlook.

II. METHODS

A. Electronic structure calculation

The electronic and magnetic properties of the studied materials are obtained from first principle calculations by applying full-relativistic multiple scattering theory as formulated in the Korringa-Kohn-Rostocker (KKR) approach⁴³. This method is implemented in the SPR-KKR package^{44,45}. Solving the Dirac equation, relativistic effects are fully accounted for, especially the spin-orbit interaction which is essential for heavy elements such as the here considered dopants Os, W, Ru , and Mo . The potentials are treated by the atomic sphere approximation (ASA) and obtained by self-consistently solving the Kohn-Sham density functional theory (DFT) equation within the local density (LDA) or generalized gradient

approximation (PBE) as devised by Perdew, Burke and Ernzerhof^{46,47}. Note that we applied the PBE functional if not further specified. The irreducible Brillouin zone is sampled by ≈ 500 k-points. To describe substitutional disorder in the sub-lattices of the alloys we make use of the coherent potential approximation (CPA)⁴⁸. The spin-polarized scalar relativistic full-potential (SR-FP) mode⁴⁹ of the KKR approach is used to calculate the total energies as a function of volume $[E(V)]$, which gives an estimate of the lattice constant a_0 .

B. Calculation of Heisenberg exchange and Gilbert damping

The angular momentum transfer in terms of Heisenberg exchange interactions J_{ij} and energy dissipation related to the Gilbert damping parameter α is determined by an ab-initio method with the aim to address the magnetic ground state and also the dynamical properties by using the Landau-Lifshitz-Gilbert equation. The interatomic exchange interactions, J_{ij} , were calculated via the Liechtenstein-Katsnelson-Antropov-Gubanov (LKAG) formalism⁵⁰

$$J_{ij} = \frac{1}{\pi} \int_{-\infty}^{\varepsilon_F} \text{Im Tr} \left(\Delta_i \tau_{ij}^\uparrow \Delta_j \tau_{ji}^\downarrow \right) d\varepsilon. \quad (1)$$

where $\Delta_i = t_{i,\uparrow}^{-1} - t_{i,\downarrow}^{-1}$ is the spin-resolved difference of the single-site scattering matrix t_i at site i and τ_{ij} is the scattering path operator, describing the propagation of the electrons between two sites i and j . The Fermi energy is denoted by ε_F . Note that in CPA, the multiple scattering matrix is replaced by the scattering properties of the effective medium $\hat{\tau}_{i\mu,j\nu} = X_{i\mu} \tau_{ij}^{CPA} X_{j\nu}$ constructed from a defect of type μ, ν at site i, j , respectively. The defects are taken into account by the defect matrix $X_{i\mu}$. From the calculated exchange interactions, it is possible to obtain the spin wave stiffness, D , which is expressed as:⁵¹

$$D = \lim_{\eta \rightarrow 0} \frac{2}{3} \sum_j e^{-\eta \frac{|\mathbf{r}_{0j}|}{a_0}} J_{0j} |\mathbf{r}_{ij}|^2 \quad (2)$$

by using super cell calculation with random configurations of the dopants in 12 ensembles and starting from a reference site $i = 0$. The distance between site i and j is given by \mathbf{r}_{ij} and the parameter η is introduced to guarantee convergence within a Pade interpolation approximation.

The Gilbert damping parameter is identified on the basis of the linear response theory³³ by means of the multiple scattering formalism⁵². The diagonal elements $\mu = x, y, z$ of the Gilbert damping tensor can be written as³³:

$$\alpha^{\mu\mu} = \frac{g}{\pi m_{tot}} \sum_j \text{Tr} \langle \mathcal{T}_0^\mu \tilde{\tau}_{0j} \mathcal{T}_j^\mu \tilde{\tau}_{j0} \rangle_c, \quad (3)$$

where the effective g-factor $g = 2(1 + m_{orb}/m_{spin})$ and total magnetic moment $m_{tot} = m_{spin} + m_{orb}$ are given by the spin and orbital moments, m_{spin} and m_{orb} , respectively, ascribed to a unit cell. Equation (3) gives $\alpha^{\mu\mu}$ for the atomic cell at lattice site 0 and implies a summation over contributions from all sites indexed by j , including $j = 0$. Moreover, $\tilde{\tau}_{ij}$ is related to the imaginary part of the multiple scattering operator that is evaluated only at the Fermi energy ε_F . Finally, \mathcal{T}_i^μ represents the matrix elements of the torque operator $\hat{\mathcal{T}}^\mu = \beta\sigma^\mu B_{xc}(\mathbf{r})$. The notation $\langle \dots \rangle_c$ represents the configurational average, including vertex corrections³³ derived by Butler⁵³ and accounting for finite temperature using the alloy analogy model within CPA⁵⁴.

C. Atomistic spin dynamics

The evolution of atomistic spins in a thermal bath is described by the Landau-Lifshitz-Gilbert (LLG) equation^{55,56}, where the dynamics of a magnetic moment is expressed in terms of precession and damping:

$$\frac{d\mathbf{m}_i(t)}{dt} = -\frac{\gamma}{(1 + \alpha^2)} \left(\mathbf{m}_i(t) \times \mathbf{B}_i(t) + \frac{\alpha}{m_i} \mathbf{m}_i(t) \times (\mathbf{m}_i(t) \times \mathbf{B}_i(t)) \right). \quad (4)$$

Here γ is the gyromagnetic ratio, α represents the dimensionless Gilbert damping constant, and $\mathbf{m}_i = m_i \mathbf{e}_i$ is an individual atomic moment on site i . The effective magnetic field is given by $\mathbf{B}_i = -\frac{\partial \mathcal{H}}{\partial \mathbf{m}_i} + \mathbf{b}_i$, where $\mathcal{H} = -\sum_{i \neq j} J_{ij} \mathbf{e}_i \cdot \mathbf{e}_j$ and \mathbf{b}_i is a stochastic field. The latter describes white noise ($\langle \mathbf{b}_i(t) \cdot \mathbf{b}_j(t') \rangle = 2D\delta_{ij}\delta(t - t')$), where the fluctuation width is $D = \alpha k_B T_s / \gamma m$. Thus, the spin temperature T_s directly passes into LLG equation via the stochastic magnetic field \mathbf{b}_i and is obtained from solving the two-temperature (2T) model⁵⁷. The analytical expression of this two temperature model reads,

$$T_s = T_0 + (T_P - T_0) \times (1 - \exp^{-t/\tau_{\text{initial}}}) \times \exp^{-t/\tau_{\text{final}}} + (T_F - T_0) \times (1 - \exp^{-t/\tau_{\text{final}}}) \quad (5)$$

where T_0 is the initial temperature of the system, T_P is the peak temperature after the laser pulse is applied and T_F is the final temperature. Both the initial and final temperature are set to 300 K, where the peak temperature is a parameter in the simulations. The time-dependent parameters τ_{initial} and τ_{final} are exponential parameters, fixed by $\tau_{\text{initial}} = 10$ fs and $\tau_{\text{final}} = 20$ ps from Ref. [58]. Note that both relaxation times are materials specific and k_B is the Boltzmann constant.

III. RESULTS AND DISCUSSION

This current section is divided in five parts. In the first and second part we discuss the electronic structure and the magnetic moments, respectively, of pure and doped Heusler and inverse Heusler materials based on DFT-optimized lattice constants. The third part deals with the Heisenberg interaction, spin wave stiffness, as well as the ordering temperature. The Gilbert damping is discussed in part four. The last part focuses on the demagnetisation and reliable switching in Heusler materials based on the LLG equation.

A. Electronic structure calculations

Lattice parameters are estimated from total energy calculations, compared to Refs. [38] and [59], and listed in Table I. For undoped Mn_2CoAl and Mn_2VAl , we improved the theoretically predicted values used in Ref. [59] by 10% and they are closer to the experimentally measured lattice constant. The improvement comes from taking into account the full-potential, which is known to improve lattice constants⁶⁰. By doping Mn with 4d and 5d metals Mo, Ru, W, and Os, we observe an expected increase of the lattice constant with the concentration of the dopants, since the atomic radius of the dopant is larger than the one of Mn. For Mn_2VAl , the increase of the lattice constant is substantially bigger ($\approx 1\%$ for $x = 1\%$ doping) than for Mn_2CoAl ($\approx 0.1\%$ for $x = 1\%$ doping).

Thermal switching within our classical atomistic model is completely determined by the Heisenberg exchange and the Gilbert damping of the system⁶¹, which are in turn identified by the scattering-path matrices and the single-site scattering matrices of the Kohn-Sham problem in Eqs. (1) and (3). Hence, we first have to address the electronic structure by means of the density of states (DOS; Fig. 2). The here studied inverse Heusler Mn_2CoAl is known to be a spin gapless semiconductor, where an almost zero-width energy gap at the Fermi level exists in the majority-spin channel (the majority states are plotted with positive values and the minority spin states with negative values) but a regular energy gap occurs in the minority spin-channel (see inset in the bottom panel of Fig. 2). This was already reported, for example, in Ref. [59]. The density of states and, consequently, the gap are sensitive to the applied exchange correlation functional. Using local density approximation (LDA), states are shifted up in energy (not shown here) compared to the PBE by about 10 meV and, consequently, no gap at the Fermi energy is observed. Note that the offset of the energy from the real axis in Fig. 2 (the spectral width of the electron bands) is small and about 1 meV, which causes sharp features in the DOS. A finite spectral width also gives rise to an overlap of the states around the Fermi level and ‘hide’ the zero-width energy gap; a finite density of states at ε_F is observed. Bands

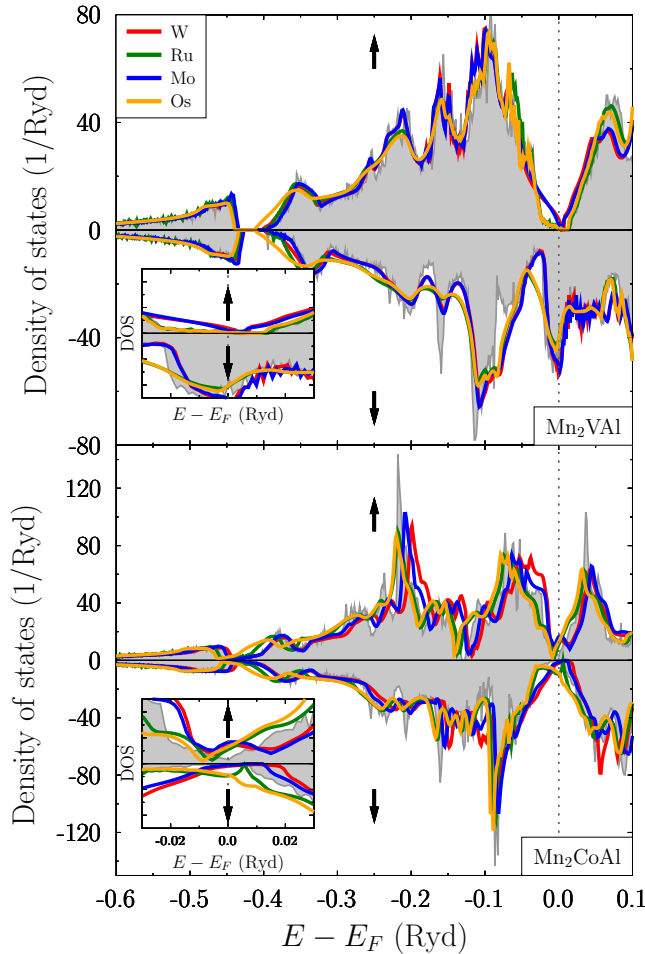


FIG. 2. (Color online) Density of states (DOS) for Mn_2CoAl (lower panel) and Mn_2VAI (upper panel) without doping (gray background) and with doping of W (red lines), Ru (blue lines), Mo (green lines), and Os (orange lines). Positive (negative) DOS values correspond to the majority-(minority-) spin electrons and are indicated by bold up-(down-) arrays. The inset is a magnification of the DOS around the Fermi level.

that cross the Fermi level, are mainly allocated to Mn^1 and Co (band structure is not shown here, but it can be found elsewhere⁴¹). Note that the superscripts 1 and 2 between the two Mn atoms. In contrast to Ref. [59], the Fermi energy is not located at the centre of the minority band gap, which will affect the coupling between the collective and single-electron excitations, i.e. the exchange interactions.

The chemical compound Mn_2VAI , however, is half-metallic (cf. Fig. 2) with a gap in the majority spin-channel. The width of the majority band gap (0.7 eV) is bigger than the minority spin gap in Mn_2CoAl (0.4 eV), which significantly affects the magnetic properties. In the minority spin channel and at the Fermi energy Mn projected states cause a strong peak in the DOS that hy-

bridize with V atoms. States above the Fermi energy are dominated by the d-states of V atoms.

The spin-gapless semiconducting or half-metallic behaviour in $\text{Mn}_{2-x}\text{Z}_x\text{CoAl}$ and $\text{Mn}_{2-x}\text{Z}_x\text{VAI}$ is destroyed by replacing some of the Mn atoms with heavy metals, $Z = \text{Mo}, \text{W}, \text{Os}, \text{Ru}$ of a given concentration $x = 0.05$ and 0.1. Comparing total energies (not shown here) allows us to conclude that for the inverse Heusler $\text{Mn}_{2-x}\text{Z}_x\text{CoAl}$ doping at both Mn-sites ($\text{Mn}^1\text{-Mn}^2$) has the lowest energy. We obtained a maximal energy difference of $\Delta E \approx 40$ meV when doping at $\text{Mn}^1\text{-Y}$, $\text{Mn}^2\text{-Y}$, or Y with 1% of the dopants W, Ru, Mo, Os. There is no major variation found in ΔE between the different dopants. Note that we used here the same lattice constant as shown in Table I, but in principle it will vary when doping at $\text{Mn}^1\text{-Mn}^2$, $\text{Mn}^1\text{-Y}$, $\text{Mn}^2\text{-Y}$, or Y. However, $\text{Mn}_{2-x}\text{Z}_x\text{VAI}$ has the lowest energy when doping only the V atom, but to treat both material on the same footing, we consider also $\text{Mn}_{2-x}\text{Z}_x\text{VAI}$ to be doped at the $\text{Mn}^1\text{-Mn}^2$ atoms.

In the case of Mn_2CoAl , W and Mo generate states at the spin-gap majority states at the Fermi level, where on the other hand the gap in the minority spin channel survives. In terms of a rigid band model, W- and Mo-doping decreases the Fermi energy, which relocates the DOS to higher energies. The dopants Os and Ru have one electron more than Mn in the valence band and, consequently, affect the density of states in the opposite way: Minority states are added and become occupied. The Fermi energy increases, which shifts the density of states to smaller energies. For Mn_2VAI , doping with Ru and Os preserves the half-metallic behaviour; it adds states below the Fermi energy and typically at the energy $\varepsilon = -0.025$ Ryd. Doping with Mo and W reduces the width of the band-gap and shifts it above the Fermi energy. Related to the alloying, the density of states smears out in the whole energy range.

B. Magnetic moments

The exchange splitting in the DOS and, consequently, the total magnetic moment is affected by doping (see Fig. 3). Both Heusler materials are ferrimagnetic. An antiferromagnetic coupling between the Mn atoms was observed for the inverse Heusler alloy Mn_2CoAl (cf. Table I), caused by the inequivalence of the two Mn atoms. These results are in good agreement with experiments^{41,42} and existing theoretical predictions^{59,62}. According to the Bethe-Slater curve⁶³, transition-metal atoms such as Mn tend to have an antiferromagnetic spin moment when they are close to each other. In $\text{Mn}_{2-x}\text{Z}_x\text{VAI}$, the Mn atoms are equivalent and, thus, have the same magnetic moment that couple ferromagnetically. The V atom, however, is antiferromagnetic with respect to the Mn atoms and has a strong induced magnetic moment of $0.91 \mu_B$. Opposite to the total magnetic moment, the size of the element resolved magnetic moments is sensitive to the lattice constant of the system

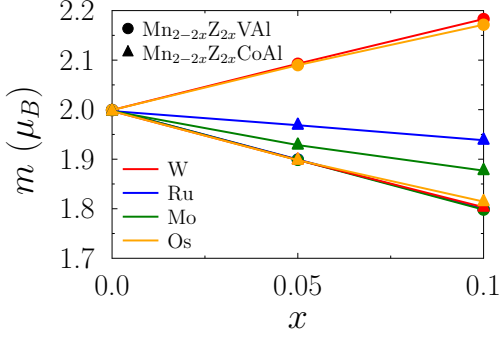


FIG. 3. (Color online) Total magnetic moments of $\text{Mn}_{2-x}\text{Z}_x\text{CoAl}$ (triangles) and $\text{Mn}_{2-x}\text{Z}_x\text{VAl}$ (circles) as a function of dopant concentration x . The symbol Z represents Mo (green lines and symbols), Os (orange lines and symbols), Ru (blue lines and symbols), and W (red lines and symbols).

and moments can vary up to 13 %, which was also found in Ref. 59.

The size but not the sign of the elemental magnetic moments changes by doping the Heusler materials with 4d and 5d heavy metals, and, thus, also the total magnetic moment. Typically, the induced magnetic moments of dopants are parallel to the magnetic moment of Mn atoms and they become larger if the magnetic moment of the Mn atom is smaller. In the case of Mn_2CoAl , the dopants W, Ru, Mo, and Os cause a decay of the total magnetic moment of about $0.1 - 0.2 \mu_B$ for $x = 1\%$, while in the case of Mn_2VAl , only the dopants Ru and Mo decrease the magnetic moment. This is caused by a significant change of the Mn magnetic moments of about $\Delta m \approx 0.1 - 0.2 \mu_B$, but also for Co atoms the moment variation is about $\Delta m \approx 0.2 \mu_B$.

C. Heisenberg exchange parameter and Curie temperatures

Based on our electronic structure analysis in the Section III B, we calculated the Heisenberg exchange parameter J_{ij} (see Fig. 4). The already revealed ferrimagnetic behaviour is reflected also in the exchange constants J . The magnetic exchange parameters decay very rapidly with the interatomic distance, r_{ij} , which is ascribed to the existence of the finite spin gap in the minority-channel^{51,64}. Our results for Mn_2CoAl are similar to the ones already reported in Refs. [62,59]. Note the factor of 2 in Ref. [59] may be caused by a different double-counting convention of the Heisenberg Hamiltonian. For the compound Mn_2CoAl , the antiferromagnetic interaction between Mn^1 and Mn^2 dominates the ferrimagnetism, whereas the Mn^2 -Co interatomic exchange interaction is ferromagnetic. In Mn_2VAl , the situation is the opposite: the Mn to V interaction is dominating and antiferromagnetic, where only the Mn^1 - Mn^2 contributes

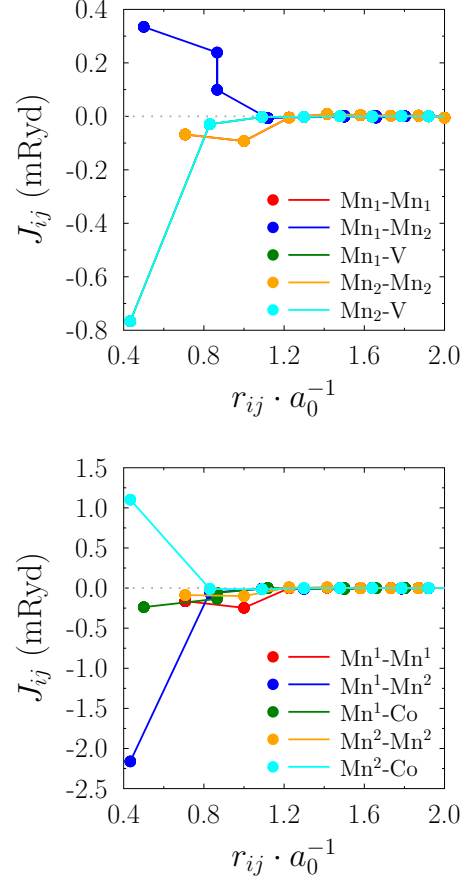


FIG. 4. (Color online) Intersublattice Heisenberg exchange parameter as a function of renormalized interatomic distance for a) Mn_2VAl and b) Mn_2CoAl . Different colours represents the coupling between Mn^1 - Mn^1 (red dots), Mn^1 - Mn^2 (blue dots), Mn^1 -Co or Mn^1 -V (green dots), Mn^2 - Mn^2 (orange dots) and Mn^2 -Co or Mn^2 -V (cyan dots).

with a ferromagnetic coupling but with half the strength of the Mn-V interaction. The coupling between equivalent Mn atoms in Mn_2VAl (Mn^1 - Mn^1 and Mn^2 - Mn^2) is small and negligible. The calculated interactions depend to some extent on the details of the calculations. In particular, the $J^{\text{Mn-Co}}$ and $J^{\text{Mn-V}}$ interactions depend strongly on the applied exchange-correlation functional, but also on the lattice constant of the system. Notice that for $J^{\text{Mn-Co}}$ and $J^{\text{Mn-V}}$ in LDA we obtain twice the size of the J 's from PBE (not shown here). The other couplings (e.g. $J^{\text{Mn-Al}}$, $J^{\text{Co-Al}}$, $J^{\text{V-Al}}$) turned out to be negligible, primarily caused by a vanishing magnetic moment on the Al atom.

As shown in Fig. 5, doping with 4d and 5d elements reduces nearest-neighbour interactions and the correlation length between magnetic moments, which is a direct consequence of the disorder and the coherent potential approximation⁶⁵. Nearest neighbour interactions are affected mostly by the doping. In general, the exchange

Compound	a_0 (Å)	$m_{[Mn^1]}$	$m_{[Z^1]}$	$m_{[Mn^2]}$	$m_{[Z^2]}$	$m_{[Y]}$
Mn ₂ CoAl	5.73 [59]	-1.64		2.77		0.93
Mn _{1.8} W _{0.2} CoAl		-1.52	-0.52	2.75	0.26	0.78
Mn _{1.8} Ru _{0.2} CoAl		-1.62	-0.10	2.76	0.06	0.91
Mn _{1.8} Mo _{0.2} CoAl		-1.53	-0.56	2.75	0.33	0.78
Mn _{1.8} Os _{0.2} CoAl		-1.56	-0.12	2.76	0.18	0.92
Mn ₂ VAl	5.69 [38]	1.32		1.32		-0.66
Mn _{1.8} W _{0.2} VAl		1.32	0.19	1.32	0.19	-0.57
Mn _{1.8} Ru _{0.2} VAl		1.31	0.08	1.31	0.08	-0.61
Mn _{1.8} Mo _{0.2} VAl		1.36	0.25	1.36	0.25	-0.58
Mn _{1.8} Os _{0.2} VAl		1.31	0.09	1.31	0.09	-0.60
Mn ₂ CoAl	5.79 [5.84 exp]	-1.81		2.91		0.96
Mn _{1.8} W _{0.2} CoAl	5.79	-1.37	-0.46	2.62	0.22	0.77
Mn _{1.8} Ru _{0.2} CoAl	5.79	-1.81	-0.10	2.90	0.07	0.96
Mn _{1.8} Mo _{0.2} CoAl	5.79	-1.71	-0.60	2.89	0.39	0.82
Mn _{1.8} Os _{0.2} CoAl	5.80	-1.80	-0.12	2.92	0.19	0.98
Mn ₂ VAl	5.84 [5.88 exp]	1.47		1.47		-0.91
Mn _{1.8} W _{0.2} VAl	5.92	1.73	0.37	1.73	0.37	-0.99
Mn _{1.8} Ru _{0.2} VAl	5.86	1.50	0.05	1.50	0.05	-0.89
Mn _{1.8} Mo _{0.2} VAl	5.91	1.72	0.45	1.72	0.45	-0.98
Mn _{1.8} Os _{0.2} VAl	5.92	1.52	0.06	1.52	0.06	-0.91

TABLE I. Lattice constant and atom resolved magnetic moments (in μ_B) of the host Mn₂CoAl and Mn₂VAl. The upper panel shows results for a fixed lattice constant obtained from literature, where the lower panel is for lattice constants calculated from total energy minimization. The superscripts 1 and 2 distinguish between the two Mn atoms. The symbol Y represents either Co or V. The magnetic moment of Al is negligibly small.

couplings diminish with doping concentration x up to 0.6 mRyd for W and $x = 0.1$. For Os and Ru doping, there is a slight increase of the exchange coupling (about 0.03 mRyd).

With knowledge about the trends in the exchange couplings $\{J\}$, one can estimate the spin-wave stiffness D and the phase transition temperature from both mean field theory via $k_B T_C^{MF} = 3/2 \sum_j J_{0j}$ or from Monte Carlo simulations. The results are shown in Fig. 6. The spin-wave stiffness (upper panel in Fig. 6) for Mn_{2-x}CoAl is in good agreement with Ref. [59], while for Mn_{2-x}VAl we reproduce the spin wave stiffness constant D already reported in Ref. [66] ($D = 324 \text{ meV}\text{\AA}^2$), but not the experimentally measured stiffness⁶⁷ ($D = 534 \text{ meV}\text{\AA}^2$). For the Co based Heusler compounds we obtain a hardening of the spin-waves after an initial softening, where for the V based Heusler compound, only hardening of the spin-waves with doping is observed. The phase transition temperature T_C , which turns out to be inversely proportional to D , decreases with doping concentration x for two reasons, namely: *i*) reduction of the magnetic moment due to doping and, consequently, stronger fluc-

tuations at a given temperature as well as *ii*) reduction of correlation. The critical temperature T_C is obtained from Monte Carlo simulations on the Metropolis algorithm⁶⁸, from Binder's fourth cumulant⁶⁸ for different simulated system sizes but also from the spin susceptibility χ . Note that the first method could fail for antiferro- and ferrimagnets. Thus, we obtain a systematic error of about ± 5 K.

Our simulations of ordering temperature (680 K for Mn₂CoAl and 475 K for Mn₂VAl) underestimate the transition temperature observed from experiment (720 K for Mn₂CoAl⁴² and 768 K for Mn₂VAl). This discrepancy that is most notable for Mn_{2-x}VAl was reported earlier⁶⁶ and could have multiple reasons. First, magnetic properties in Heusler alloys are sensitive to the interstitial region spanned by the muffin tin potential. Thus, full-potential simulations are required as it was shown in Refs. [41, 42, and 69]. Also the results depend crucially on the choice of the exchange-correlation functional and on electron correlations e.g. addressed by including a Hubbard U ⁶⁶. Second, the Heisenberg exchange is calculated for a collinear ferrimagnetic state but when the magnetic

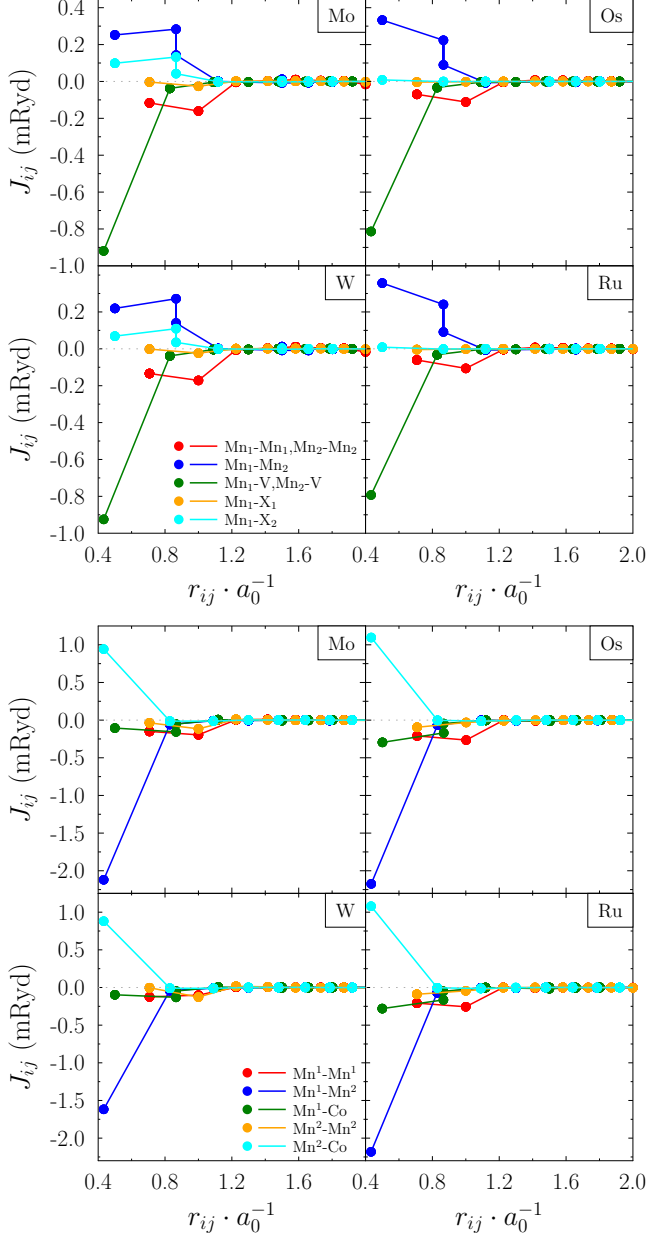


FIG. 5. (Color online) Intersublattice Heisenberg exchange parameter as a function of renormalized interatomic distance for a) $\text{Mn}_{2-x}\text{Z}_x\text{VAL}$ and b) $\text{Mn}_{2-x}\text{Z}_x\text{CoAl}$, where the different subpanels show the dopants W (bottom left), Ru (bottom right), Mo (top left), and Os (top right). Different colours represents the coupling between $\text{Mn}^1\text{-Mn}^1$ (red dots), $\text{Mn}^1\text{-Mn}^2$ (blue dots), $\text{Mn}^1\text{-Co}$ or $\text{Mn}^1\text{-V}$ (green dots), $\text{Mn}^2\text{-Mn}^2$ (orange dots) and $\text{Mn}^2\text{-Co}$ or $\text{Mn}^2\text{-V}$ (cyan dots).

disorder is taken into account in the electronic structure, usually the exchange interaction is biased⁶⁵. Based on the alloy analogy model⁵⁴, we modelled also the temperature stability of the magnetic properties (magnetic moments and magnetic exchange) coming from electronic structure by the partial disordered local moment (DLM)

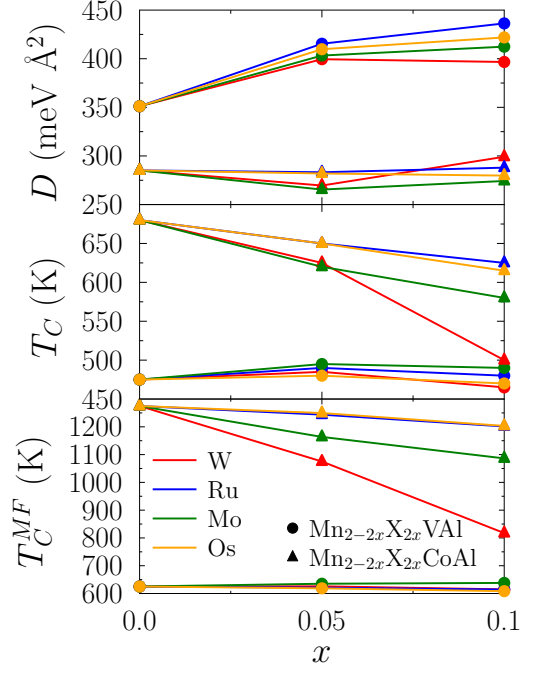


FIG. 6. (Color online) Spin wave stiffness D , critical temperatures T_C , and mean field critical temperatures T_C^{MF} of $\text{Mn}_{2-x}\text{Z}_x\text{CoAl}$ (triangles) and $\text{Mn}_{2-x}\text{Z}_x\text{VAL}$ (circles) as a function of dopand concentration x . Dopands are Mn (black circles), Os (red squares), Ru (green diamonds), and W (orange triangles).

approximation within the Ising model⁶⁵. DLM approach is believed to accurately describe ‘spin temperature’ in the electronic structure⁷⁰. However, it turned out that the disordered local moment theory can not be applied to both Heusler and inverse Heusler for similar reasons as for Ni⁷¹: the magnetic moments in Al and Co/V disappear. For Mn_2CoAl , our simulations show furthermore that the magnetic moment of the Mn^2 atom is zero in the paramagnetic phase and, consequently, the magnetic exchange and the phase transition temperature are zero. This result is independent of the doping with 4d and 5d elements. These results indicate the inconsistency of the DLM model for Heusler materials. It is still an open question, if results get improved by applying relativistic DLM theory⁷². Third, we consider only a simplified approach for electron correlation in the LDA and GGA density functional. However, it is known⁶⁶ that improved models for electron correlation have the trend to increase slightly the phase transition temperature.

D. Gilbert damping

Previous studies⁶¹ have shown that Gilbert damping is a crucial parameter in the ultrafast switching procedure and, thus, call for ab-initio footing. Figure 7 shows the

Gilbert damping α as a function x at $T = 300$ K. Note that for these calculations both lattice and magnetic fluctuations terms are considered, where the magnetic fluctuations are assumed from a linear correlation between the magnetization and the temperature. This could result in errors, in particular at high temperatures.

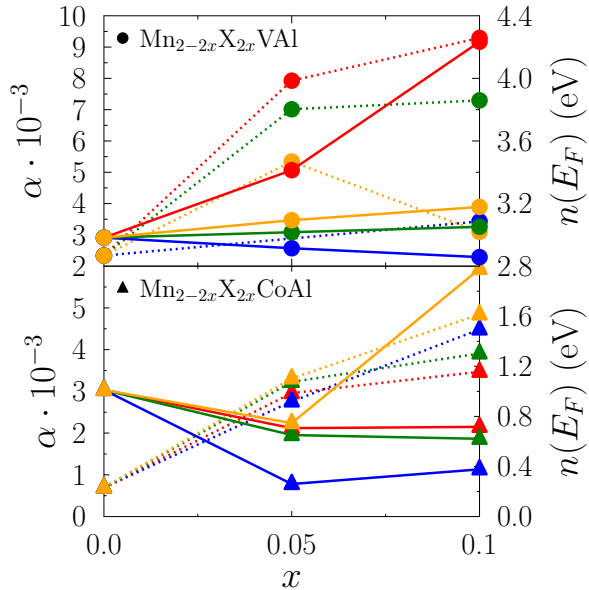


FIG. 7. (Color online) Gilbert damping parameters α (solid lines) and density of states at the Fermi level $n(E_F)$ (dotted lines) of $\text{Mn}_{2-x}\text{Z}_x\text{CoAl}$ (triangular symbols) and $\text{Mn}_{2-x}\text{Z}_x\text{VAl}$ (circle symbols) vs dopant concentration x . Dopants are W (red color), Ru (blue color), Mo (green color), and Os (orange color).

The Gilbert damping of both undoped Heusler materials (Mn_2CoAl : $\alpha = 0.0030$, Mn_2VAl : $\alpha = 0.0029$) is high compared to other half-metals reported, e.g., in Ref. [66] or low-damping alloys like $\text{Fe}_{0.75}\text{Co}_{0.25}$ ⁷³. The trends of the Gilbert damping parameters with dopant concentration are different for Heusler and inverse Heusler materials. In $\text{Mn}_{2-x}\text{Z}_x\text{VAl}$, doping leads to an increase of the damping with x , except for the case of Ru. The slope of α versus concentration x follows the general increase of the total density of states at the Fermi level as it is proposed in Refs. [33, 73, and 74], but not linear to it. This non-linearity was already observed for Heusler materials in Ref. [66] or doped permalloy with the heavy 4d and 5d elements used here⁷⁵. The observed damping α is different from zero, however, small. This is in line with the theory proposed in Ref. [74], in which damping is proportional to the product of the spin-polarised DOS and, consequently $\alpha \approx 0$. The increase of damping can be also understood in terms of the Kamberský model^{76,77}: Alloying broadens the electron bands and more spin-flip transitions between the electron states occur. This is true only, if interband transitions are already dominating. In the inverse Heusler material Mn_2CoAl we even find a decrease with x . This is due to the spin-gapless

semiconducting behaviour (cf. Fig. 2): Only a low number of states exist at the Fermi energy, making interband transitions unlikely. The damping is dominated by intra-band transitions, that tend to decrease with very small x . With increasing x , however, states appear within the gap and interband transition are preferred. Thus, a small increase with even higher concentration is expected and observed. However, not only the number of states at the Fermi energy and the spectral width of the states contribute to the damping, but also the spin-orbit coupling (SOC), the Landé factor, and the saturation magnetization affect the damping parameter. Since we dope with rather heavy elements W, Mo, Ru, and Os, spin orbit coupling strongly contributes to the variation of damping with concentration x : the higher the ‘mass’ of the dopant atom (W and Os compared to Ru and Mo) is, the higher is the damping parameter.

After we addressed all relevant parameters for the simulation based on the Landau-Lifshitz-Gilbert equation, we are able to perform ultrafast switching calculations.

E. Ultrafast switching

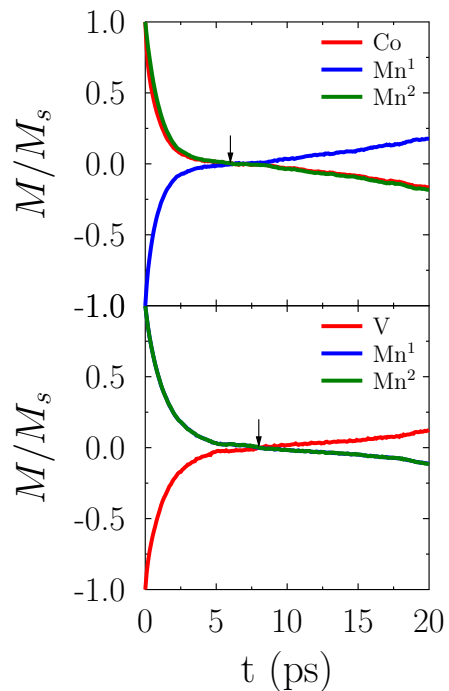


FIG. 8. (Color online) Ultrafast switching behaviour of Mn_2CoAl (upper panel) and Mn_2VAl (lower panel). The demagnetization is shown element resolved (blue and green lines - Mn atoms, red line - Co/ V atom). The peak temperature is 600 K for Mn_2VAl and 900 K for Mn_2CoAl . The external magnetic field is $B = 2.5$ T and damping parameter is $\alpha = 0.009$. The arrow indicates the crossing point at where the switching takes place.

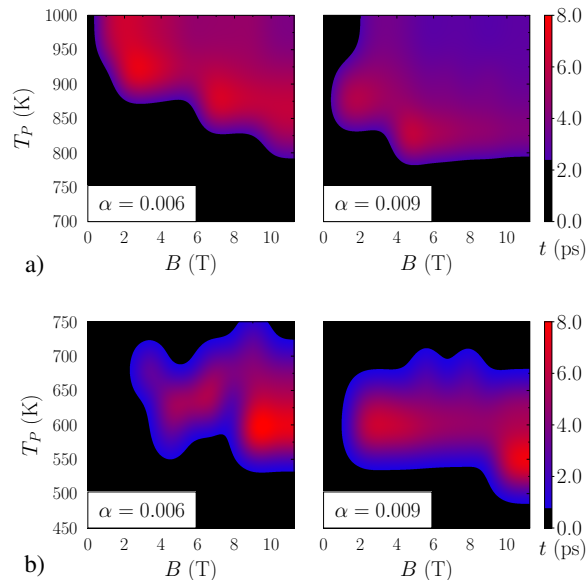


FIG. 9. (Color online) Thermal switching phase diagram for different damping parameter (0.006 and 0.009) in a) Mn_2CoAl and b) Mn_2VAl . The peak temperature is represented versus the strength of the external magnetic field. The colour scale (fast switching - blue colour, slow switching - red colour) represents the time in units of ps where the switching (indicated by an arrow in Fig. (8)) takes place. No switching is represented by the black background.

In order to study the ultrafast switching process in Heusler alloys we combined the two temperature model with an atomistic spin dynamics code⁷⁸. Here, we considered a very long thermal pulse of 20 ps with different peak temperatures T_P . Typical timescales of the ultrafast demagnetization and remagnetization process for Mn_2VAl and Mn_2CoAl are in the orders of picoseconds (1 – 5 ps) (see Fig. 8). The time scales are mainly dictated by the Gilbert damping α , which is varied in our studies between 0.003, 0.006, and 0.009, but can depend on the Heisenberg exchange¹². As demonstrated above, these damping values are achievable by doping the ‘pure’ Heusler materials. There is only a slight shift observable in the demagnetization time of each individual element in Mn_2CoAl , where for Mn_2VAl , it is not. After demagnetization, the Heusler material undergoes reliable switching only when an external magnetic field induced by the pump-pulse is present. Thus, three parameters — damping, peak temperature and pulse induced external magnetic field — span a phase space for observing reliable switching, as shown in Fig. 9.

We did not observe any magnetic switching for both Heusler materials with $\alpha = 0.003$ (data not shown here). Typically for certain threshold peak temperatures T_P above the magnetic phase transition temperature ($T_C = 700$ K for Mn_2CoAl and $T_C = 475$ K for Mn_2VAl) switching occurs. The peak temperature can be tuned by the laser intensity and the pulse duration. The presence of an effective magnetic field during pumping is discussed

in literature^{79,80}. It was argued that the electric field of the pump pulse induces a strong material specific magnetic field of 10 – 100 T. Even below but above certain minimum magnetic field of 1 – 2 T, we observed reliable switching. This threshold magnetic field as well as the switching time (indicated by reduced contrast in Fig. 9) decreases with increasing damping. The time when the switching occurs (crossing point in Fig. 8 and colour scale in Fig. 9) typically passes a maximum at certain and decreases for larger peak temperatures. However, there is also a minimum switching time of around 2 – 3 ps, controlled by the demagnetization rate. Note that due to the different spin polarization and resulting different atomic magnetic moments and magnetic states, an asymmetry in the phase diagram between Mn_2CoAl and Mn_2VAl occurs.

Nevertheless, our approach has certain limitations. For instance, we explicitly neglect the electronic motion and effects like super diffusion or spin-flip scattering, as discussed in Ref.²⁵. We also assume the damping to be ‘spin- and phonon-temperature’ independent. This is a rough approximation, in particular, due to the important role of phonons in the demagnetization process (e.g. Ref. [81]) and for energy dissipation in magnetic systems³³. Furthermore, we neglect the change of the magnetic exchange interaction with temperature, although magnetic moments of Co and V atoms vanish in the DLM approximation. This behaviour in the disordered local moment theory is well studied⁷¹ and occurs also for Ni atoms. But we have shown elsewhere⁵⁸ but also others^{82–84}, that our methodology is applicable for demagnetization in bulk bcc Fe and hcp Co compounds and, likely, for the Heusler materials studied here. We also neglect possible structural phase transition to A2 or B2 disorder during demagnetization.

IV. CONCLUSION

We have demonstrated thermal switching in Heusler and inverse Heusler materials making use of magnetic field pulse induced by the pump-pulse. We found a sensitive dependence of the possible switching and the switching time on the magnetic field pulse strength, the peak temperature in the effective two-temperature model as well as intrinsic materials properties, say the Heisenberg exchange and the Gilbert damping parameter. We have shown that the latter can be tuned by doping heavy elements, say W, Mo, Ru, Os, to both, higher and lower damping values, especially in the case of spin-gapless semiconductor. This calls for further investigations on other spin-gapless semiconductor⁵⁹, aiming for tuning the Gilbert damping to very low values, which may enable interesting spintronic and magnonic applications⁸⁵. Within our methodology, we could reproduce exchange parameter and, consequently, phase transition temperatures reported in literature⁵⁹. Our overall finding extends with Heusler and inverse Heusler alloys the class of materials

that exhibits laser induced magnetic switching and calls for future theoretical and experimental studies.

V. ACKNOWLEDGEMENT

We acknowledge financial support from the Swedish Research Council. O.E. and E.K.D.-Cz. acknowledged support from KAW (projects 2013.0020 and 2012.0031) as well as acknowledges eSENCE and STandUP. The calculations were performed at NSC (Linköping University, Sweden) under a SNAC project.

-
- ¹ E. Beaurepaire, J. C. Merle, A. Daunois, and J. Y. Bigot, Phys. Rev. Lett. **76**, 4250 (1996), URL <https://link.aps.org/doi/10.1103/PhysRevLett.76.4250>.
 - ² E. Carpenne, E. Mancini, C. Dallera, M. Brenna, E. Puppin, and S. De Silvestri, Phys. Rev. B **78**, 174422 (2008), URL <https://link.aps.org/doi/10.1103/PhysRevB.78.174422>.
 - ³ M. Cinchetti, M. S. Albaneda, D. Hoffmann, T. Roth, J. P. Wüstenberg, M. Krauß, O. Andreyev, H. C. Schneider, M. Bauer, and M. Aeschlimann, Phys. Rev. Lett. **97**, 177201 (2006), URL <https://link.aps.org/doi/10.1103/PhysRevLett.97.177201>.
 - ⁴ C. Stamm, T. Kachel, N. Pontius, R. Mitzner, T. Quast, K. Holldack, S. Khan, C. Lupulescu, E. F. Aziz, M. Wietstruck, et al., Nature Materials **6**, 740 (2007), URL http://adsabs.harvard.edu/cgi-bin/nph-data_query?bibcode=2007NatMa...6..740S&link_type=EJOURNAL.
 - ⁵ H. S. Rhie, H. A. Dürr, and W. Eberhardt, Phys. Rev. Lett. **90**, 247201 (2003), URL <https://link.aps.org/doi/10.1103/PhysRevLett.90.247201>.
 - ⁶ M. Wietstruck, A. Melnikov, C. Stamm, T. Kachel, N. Pontius, M. Sultan, C. Gahl, M. Weinelt, H. A. Dürr, and U. Bovensiepen, Phys. Rev. Lett. **106**, 127401 (2011), URL <https://link.aps.org/doi/10.1103/PhysRevLett.106.127401>.
 - ⁷ C. D. Stanciu, A. V. Kimel, F. Hansteen, A. Tsukamoto, A. Itoh, A. Kirilyuk, and T. Rasing, Phys. Rev. B **73**, 220402 (2006), URL <https://link.aps.org/doi/10.1103/PhysRevB.73.220402>.
 - ⁸ K. Vahaplar, A. M. Kalashnikova, A. V. Kimel, D. Hinzke, U. Nowak, R. Chantrell, A. Tsukamoto, A. Itoh, A. Kirilyuk, and T. Rasing, Phys. Rev. Lett. **103**, 117201 (2009), URL <https://link.aps.org/doi/10.1103/PhysRevLett.103.117201>.
 - ⁹ C. D. Stanciu, F. Hansteen, A. V. Kimel, A. Kirilyuk, A. Tsukamoto, A. Itoh, and T. Rasing, Phys. Rev. Lett. **99**, 047601 (2007), URL <https://link.aps.org/doi/10.1103/PhysRevLett.99.047601>.
 - ¹⁰ D. Steil, S. Alebrand, A. Hassdenteufel, M. Cinchetti, and M. Aeschlimann, Phys. Rev. B **84**, 224408 (2011), URL <https://link.aps.org/doi/10.1103/PhysRevB.84.224408>.
 - ¹¹ T. A. Ostler, J. Barker, R. F. L. Evans, R. W. Chantrell, U. Atxitia, O. Chubykalo-Fesenko, S. El Moussaoui, L. Le Guyader, E. Mengotti, L. J. Heyderman, et al., Nat Comms **3**, 666 (2012), URL <https://www.nature.com/articles/ncomms1666>.
 - ¹² J. H. Mentink, J. Hellsvik, D. V. Afanasiev, B. A. Ivanov, A. Kirilyuk, A. V. Kimel, O. Eriksson, M. I. Katsnelson, and T. Rasing, Phys. Rev. Lett. **108**, 057202 (2012), URL <https://link.aps.org/doi/10.1103/PhysRevLett.108.057202>.
 - ¹³ R. Chimata, L. Isaeva, K. Kádas, A. Bergman, B. Sanyal, J. H. Mentink, M. I. Katsnelson, T. Rasing, A. Kirilyuk, A. Kimel, et al., Phys. Rev. B **92**, 094411 (2015), URL <https://link.aps.org/doi/10.1103/PhysRevB.92.094411>.
 - ¹⁴ S. Alebrand, U. Bierbrauer, M. Hehn, M. Gottwald, O. Schmitt, D. Steil, E. E. Fullerton, S. Mangin, M. Cinchetti, and M. Aeschlimann, Phys. Rev. B **89**, 144404 (2014), URL <https://link.aps.org/doi/10.1103/PhysRevB.89.144404>.
 - ¹⁵ J.-Y. Bigot, M. Vomir, and E. Beaurepaire, Nat Phys **5**, 515 (2009), URL <https://www.nature.com/articles/nphys1285>.
 - ¹⁶ G. M. Müller, J. Walowski, M. Djordjevic, G.-X. Miao, A. Gupta, A. V. Ramos, K. Gehrke, V. Moshnyaga, K. Samwer, J. Schmalhorst, et al., Nature Publishing Group **8**, 56 (2008), URL <https://www.nature.com/articles/nmat2341>.
 - ¹⁷ J. P. Wüstenberg, D. Steil, S. Alebrand, T. Roth, M. Aeschlimann, and M. Cinchetti, Phys. Status Solidi B **248**, 2330 (2011), URL <http://onlinelibrary.wiley.com/doi/10.1002/pssb.201147087/full>.
 - ¹⁸ A. Mann, J. Walowski, M. Münzenberg, S. Maat, M. J. Carey, J. R. Childress, C. Mewes, D. Ebke, V. Drewello, G. Reiss, et al., Phys. Rev. X **2**, 041008 (2012), URL <https://link.aps.org/doi/10.1103/PhysRevX.2.041008>.
 - ¹⁹ D. Steil, S. Alebrand, T. Roth, M. Krauß, T. Kubota, M. Oogane, Y. Ando, H. C. Schneider, M. Aeschlimann, and M. Cinchetti, Phys. Rev. Lett. **105**, 217202 (2010), URL <https://link.aps.org/doi/10.1103/PhysRevLett.105.217202>.
 - ²⁰ Y. Liu, L. R. Sheldford, V. V. Kruglyak, R. J. Hicken, Y. Sakuraba, M. Oogane, and Y. Ando, Phys. Rev. B **81**, 094402 (2010), URL <https://link.aps.org/doi/10.1103/PhysRevB.81.094402>.
 - ²¹ B. Koopmans, G. Malinowski, F. D. Longa, D. Steiauf, M. Fähnle, T. Roth, M. Cinchetti, and M. Aeschlimann, Nature Publishing Group **9**, 259 (2009), URL <https://www.nature.com/articles/nmat2593>.
 - ²² I. Radu, K. Vahaplar, C. Stamm, T. Kachel, N. Pontius, H. A. Dürr, T. A. Ostler, J. Barker, R. F. L. Evans, R. W. Chantrell, et al., Nature **472**, 205 (2011), URL <https://www.nature.com/articles/nature09901>.
 - ²³ N. Kazantseva, U. Nowak, R. W. Chantrell, J. Hohlfield, and A. Rebei, EPL **81**, 27004 (2008), URL <http://iopscience.iop.org/article/10.1209/0295-5075/81/27004>.
 - ²⁴ U. Atxitia, O. Chubykalo-Fesenko, N. Kazantseva, D. Hinzke, U. Nowak, and R. W. Chantrell, Applied

- Physics Letters **91**, 232507 (2007), URL <http://aip.scitation.org/doi/10.1063/1.2822807>.
- ²⁵ M. Battiato, K. Carva, and P. M. Oppeneer, Phys. Rev. Lett. **105**, 027203 (2010), URL <https://link.aps.org/doi/10.1103/PhysRevLett.105.027203>.
 - ²⁶ A. Melnikov, I. Razdolski, T. O. Wehling, E. T. Papaioannou, V. Roddatis, P. Fumagalli, O. Aktsipetrov, A. I. Lichtenstein, and U. Bovensiepen, Phys. Rev. Lett. **107**, 076601 (2011), URL <https://link.aps.org/doi/10.1103/PhysRevLett.107.076601>.
 - ²⁷ K. Carva, M. Battiato, and P. M. Oppeneer, Phys. Rev. Lett. **107**, 207201 (2011), URL <https://link.aps.org/doi/10.1103/PhysRevLett.107.207201>.
 - ²⁸ S. Essert and H. C. Schneider, Phys. Rev. B **84**, 224405 (2011), URL <https://link.aps.org/doi/10.1103/PhysRevB.84.224405>.
 - ²⁹ U. Atxitia and O. Chubykalo-Fesenko, Phys. Rev. B **84**, 144414 (2011), URL <https://link.aps.org/doi/10.1103/PhysRevB.84.144414>.
 - ³⁰ M. Fähnle and C. Illg, J. Phys.: Condens. Matter **23**, 493201 (2011), URL <http://iopscience.iop.org/article/10.1088/0953-8984/23/49/493201>.
 - ³¹ K. Gilmore, Y. U. Idzerda, and M. D. Stiles, Phys. Rev. Lett. **99**, 027204 (2007), URL <https://link.aps.org/doi/10.1103/PhysRevLett.99.027204>.
 - ³² A. Brataas, Y. Tserkovnyak, and G. E. W. Bauer, Phys. Rev. Lett. **101**, 037207 (2008), URL <https://link.aps.org/doi/10.1103/PhysRevLett.101.037207>.
 - ³³ H. Ebert, S. Mankovsky, D. Ködderitzsch, and P. J. Kelly, Phys. Rev. Lett. **107**, 066603 (2011), URL <http://link.aps.org/doi/10.1103/PhysRevLett.107.066603>.
 - ³⁴ H. Itoh, T. Nakamichi, Y. Yamaguchi, and N. Kazama, Transactions of the Japan Institute of Metals **24**, 265 (1983), URL https://www.jstage.jst.go.jp/article/matertrans1960/24/5/24_5_265/_article.
 - ³⁵ Y. Yutaka, K. Masayuki, and N. Takuro, J. Phys. Soc. Jpn. **50**, 2203 (2013), URL <http://journals.jps.jp/doi/10.1143/JPSJ.50.2203>.
 - ³⁶ C. Jiang, M. Venkatesan, and J. M. D. Coey, Solid State Communications **118**, 513 (2001), URL <http://linkinghub.elsevier.com/retrieve/pii/S003810980100151X>.
 - ³⁷ I. Shoji, A. Setsuro, and I. Junji, J. Phys. Soc. Jpn. **53**, 2718 (2013), URL <http://journals.jps.jp/doi/10.1143/JPSJ.53.2718>.
 - ³⁸ K. Özdoğan, I. Galanakis, E. Şaşıoğlu, and B. Aktaş, J. Phys.: Condens. Matter **18**, 2905 (2006), URL <http://iopscience.iop.org/article/10.1088/0953-8984/18/10/013>.
 - ³⁹ E. Şaşıoğlu, L. M. Sandratskii, and P. Bruno, J. Phys.: Condens. Matter **17**, 995 (2005), URL <http://iopscience.iop.org/article/10.1088/0953-8984/17/6/017>.
 - ⁴⁰ R. Weht and W. E. Pickett, Phys. Rev. B **60**, 13006 (1999), URL <https://link.aps.org/doi/10.1103/PhysRevB.60.13006>.
 - ⁴¹ G. D. Liu, X. F. Dai, H. Y. Liu, J. L. Chen, Y. X. Li, G. Xiao, and G. H. Wu, Phys. Rev. B **77**, 014424 (2008), URL <https://link.aps.org/doi/10.1103/PhysRevB.77.014424>.
 - ⁴² S. Ouardi, G. H. Fecher, C. Felser, and J. Kübler, Phys. Rev. Lett. **110**, 100401 (2013), URL <https://link.aps.org/doi/10.1103/PhysRevLett.110.100401>.
 - ⁴³ J. Zablouil, L. Szunyogh, R. Hammerling, and P. Weinberger, *Electron Scattering in Solid Matter*, A Theoretical and Computational Treatise (2006), URL <http://bookzz.org/md5/190C5DE184B30E2B6898DE499DFB7D78>.
 - ⁴⁴ H. Ebert, D. Ködderitzsch, and J. Minár, Rep. Prog. Phys. **74**, 096501 (2011), URL <http://iopscience.iop.org/article/10.1088/0034-4885/74/9/096501>.
 - ⁴⁵ H. Ebert, *The Munich SPR-KKR package, version 6.3*, (2012), URL <http://ebert.cup.uni-muenchen.de/SPRKKR>.
 - ⁴⁶ E. K. U. Gross and R. M. Dreizler, *Density Functional Theory* (Springer Science & Business Media, 2013), ISBN 1475799756, URL http://books.google.se/books?id=aG4ECAAQBAJ&pg=PR4&dq=10.1007/978-1-4757-9975-0&hl=&cd=1&source=gbps_api.
 - ⁴⁷ J. P. Perdew, K. Burke, and M. Ernzerhof, Phys. Rev. Lett. **77**, 3865 (1996), URL <https://link.aps.org/doi/10.1103/PhysRevLett.77.3865>.
 - ⁴⁸ B. L. Gyorffy, Phys. Rev. B **5**, 2382 (1972), URL <https://link.aps.org/doi/10.1103/PhysRevB.5.2382>.
 - ⁴⁹ T. Hühne, C. Zecha, H. Ebert, P. H. Dederichs, and R. Zeller, Physical Review B (Condensed Matter and Materials Physics) **58**, 10236 (1998), URL http://adsabs.harvard.edu/cgi-bin/nph-data_query?bibcode=1998PhRvB..58I0236H&link_type=EJOURNAL.
 - ⁵⁰ A. I. Liechtenstein, M. I. Katsnelson, and V. A. Gubanov, J. Phys. F: Met. Phys. **14**, L125 (1984), URL <http://iopscience.iop.org/article/10.1088/0305-4608/14/7/007>.
 - ⁵¹ M. Pajda, J. Kudrnovský, I. Turek, V. Drchal, and P. Bruno, Phys. Rev. B **64**, 174402 (2001), URL <https://link.aps.org/doi/10.1103/PhysRevB.64.174402>.
 - ⁵² S. Mankovsky, D. Ködderitzsch, G. Woltersdorf, and H. Ebert, Phys. Rev. B **87**, 014430 (2013), URL <https://link.aps.org/doi/10.1103/PhysRevB.87.014430>.
 - ⁵³ W. H. Butler, Phys. Rev. B **31**, 3260 (1985), URL <https://link.aps.org/doi/10.1103/PhysRevB.31.3260>.
 - ⁵⁴ H. Ebert, S. Mankovsky, K. Chadova, S. Polesya, J. Minár, and D. Ködderitzsch, Phys. Rev. B **91**, 165132 (2015), URL <https://link.aps.org/doi/10.1103/PhysRevB.91.165132>.
 - ⁵⁵ V. P. Antropov, M. I. Katsnelson, B. N. Harmon, M. van Schilfgaarde, and D. Kusnezov, Phys. Rev. B **54**, 1019 (1996), URL <https://link.aps.org/doi/10.1103/PhysRevB.54.1019>.
 - ⁵⁶ O. Eriksson, A. Bergman, L. Bergqvist, and J. Hellsvik, *Atomistic Spin Dynamics*, Foundations and Applications (Oxford University Press, 2016), URL <https://global.oup.com/academic/product/atomistic-spin-dynamics-9780198788669>.
 - ⁵⁷ U. Bovensiepen, J. Phys.: Condens. Matter **19**, 083201 (2007), URL <http://iopscience.iop.org/article/10.1088/0953-8984/19/8/083201>.
 - ⁵⁸ R. Chimata, A. Bergman, L. Bergqvist, B. Sanyal, and O. Eriksson, Phys. Rev. Lett. **109**, 157201 (2012), URL <https://link.aps.org/doi/10.1103/PhysRevLett.109.157201>.
 - ⁵⁹ A. Jakobsson, P. Mavropoulos, E. Şaşıoğlu, S. Blügel, M. Ležaić, B. Sanyal, and I. Galanakis, Phys. Rev. B **91**, 174439 (2015), URL <https://link.aps.org/doi/10.1103/PhysRevB.91.174439>.
 - ⁶⁰ K. Motizuki, H. Ido, T. Itoh, and M. Morifuji, *Electronic Structure and Magnetism of 3d-Transition Metal Pnictides* (Springer Science &

- Business Media, 2009), ISBN 3642034209, URL http://books.google.se/books?id=g1wv4vHY58cC&printsec=frontcover&dq=intitle:Electronic+Structure+and+Magnetism+of+3d+Transition+Metal+Kazuko+Motizuki+Springer&hl=&cd=1&source=gbp_api.
- ⁶¹ R. Chimata, E. K. Delczeg-Czirjak, A. Szilva, R. Cardias, Y. O. Kvashnin, M. Pereiro, S. Mankovsky, H. Ebert, D. Thonig, B. Sanyal, et al., Phys. Rev. B **95**, 214417 (2017), URL <http://link.aps.org/doi/10.1103/PhysRevB.95.214417>.
 - ⁶² M. Meinert, J.-M. Schmalhorst, and G. Reiss, J. Phys.: Condens. Matter **23**, 116005 (2011), URL <http://iopscience.iop.org/article/10.1088/0953-8984/23/11/116005>.
 - ⁶³ D. Jiles, *Introduction to Magnetism and Magnetic Materials, Third Edition* (CRC Press, 2015), ISBN 1482238888, URL http://books.google.se/books?id=2diYCGAAQBAJ&printsec=frontcover&dq=intitle:Introduction+to+Magnetism+and+Magnetic+Materials+Second+Edition&hl=&cd=1&source=gbp_api.
 - ⁶⁴ J. Rusz, L. Bergqvist, J. Kudrnovský, and I. Turek, Phys. Rev. B **73**, 214412 (2006), URL <https://link.aps.org/doi/10.1103/PhysRevB.73.214412>.
 - ⁶⁵ D. Böttcher, A. Ernst, and J. Henk, Journal of Magnetism and Magnetic Materials **324**, 610 (2012), URL <http://linkinghub.elsevier.com/retrieve/pii/S0304885311006299>.
 - ⁶⁶ J. Chico, S. Keshavarz, Y. Kvashnin, M. Pereiro, I. Di Marco, C. Etz, O. Eriksson, A. Bergman, and L. Bergqvist, Phys. Rev. B **93**, 214439 (2016), URL <https://link.aps.org/doi/10.1103/PhysRevB.93.214439>.
 - ⁶⁷ R. Y. Umetsu and T. Kanomata, Physics Procedia **75**, 890 (2015), URL <http://linkinghub.elsevier.com/retrieve/pii/S187538921501754X>.
 - ⁶⁸ K. Binder and D. Heermann, *Monte Carlo Simulation in Statistical Physics*, vol. 5 of *An Introduction* (Berlin Heidelberg, 2010), springer-verlag ed., URL <http://www.springer.com/de/book/9783642031625>.
 - ⁶⁹ K. Meinel, A. Beckmann, M. Klaua, and H. Bethge, physica status solidi (a) **150**, 521 (1995), URL <http://doi.wiley.com/10.1002/pssa.2211500146>.
 - ⁷⁰ J. Staunton, *Relativistic Effects and Disordered Local Moments in Magnets* (2013), URL http://www.psi-k.org/newsletters/News_82/Highlight_82.pdf.
 - ⁷¹ H. Akai and P. H. Dederichs, Phys. Rev. B **47**, 8739 (1993), URL <https://link.aps.org/doi/10.1103/PhysRevB.47.8739>.
 - ⁷² A. Buruzs, Ph.D. thesis, cms.tuwien.ac.at, Wien (2008), URL <http://www.cms.tuwien.ac.at/media/pdf/phd-thesis/THESIS.PDF>.
 - ⁷³ M. A. W. Schoen, D. Thonig, M. L. Schneider, T. J. Silva, H. T. Nembach, O. Eriksson, O. Karis, and J. M. Shaw, Nat Phys **12**, 839 (2016), URL <http://www.nature.com/doi/10.1038/nphys3770>.
 - ⁷⁴ S. Lounis, M. dos Santos Dias, and B. Schweglinghaus, Phys. Rev. B **91**, 104420 (2015), URL <https://link.aps.org/doi/10.1103/PhysRevB.91.104420>.
 - ⁷⁵ F. Pan, J. Chico, J. Hellsvik, A. Delin, A. Bergman, and L. Bergqvist, Phys. Rev. B **94**, 214410 (2016), URL <https://link.aps.org/doi/10.1103/PhysRevB.94.214410>.
 - ⁷⁶ V. Kamberský, Czech J Phys **34**, 1111 (1984), URL <https://link.springer.com/article/10.1007/BF01590106>.
 - ⁷⁷ V. Kamberský, Czech J Phys **26**, 1366 (1976), URL <http://link.springer.com/10.1007/BF01587621>.
 - ⁷⁸ B. Skubic, J. Hellsvik, L. Nordström, and O. Eriksson, J. Phys.: Condens. Matter **20**, 315203 (2008), URL <http://iopscience.iop.org/article/10.1088/0953-8984/20/31/315203>.
 - ⁷⁹ M. Berritta, R. Mondal, K. Carva, and P. M. Oppeneer, Phys. Rev. Lett. **117**, 137203 (2016), URL <https://link.aps.org/doi/10.1103/PhysRevLett.117.137203>.
 - ⁸⁰ R. John, M. Berritta, D. Hinzke, C. Müller, T. Santos, H. Ulrichs, P. Nieves, J. Walowski, R. Mondal, O. Chubykalo-Fesenko, et al., Sci. Rep. **7**, 4114 (2017), URL http://adsabs.harvard.edu/cgi-bin/nph-data_query?bibcode=2017NatSR...7.4114J&link_type=EJOURNAL.
 - ⁸¹ C. Illg, M. Haag, and M. Fähnle, Phys. Rev. B **88**, 214404 (2013), URL <https://link.aps.org/doi/10.1103/PhysRevB.88.214404>.
 - ⁸² R. F. L. Evans, U. Atxitia, and R. W. Chantrell, Phys. Rev. B **91**, 144425 (2015), URL <https://link.aps.org/doi/10.1103/PhysRevB.91.144425>.
 - ⁸³ D. Hinzke, U. Atxitia, K. Carva, P. Nieves, O. Chubykalo-Fesenko, P. M. Oppeneer, and U. Nowak, Phys. Rev. B **92**, 259 (2015), URL <https://link.aps.org/doi/10.1103/PhysRevB.92.054412>.
 - ⁸⁴ U. Atxitia, D. Hinzke, O. Chubykalo-Fesenko, U. Nowak, H. Kachkachi, O. N. Mryasov, R. F. Evans, and R. W. Chantrell, Phys. Rev. B **82**, 134440 (2010), URL <https://link.aps.org/doi/10.1103/PhysRevB.82.134440>.
 - ⁸⁵ C. J. Palmström, Progress in Crystal Growth and Characterization of Materials **62**, 371 (2016), URL <http://linkinghub.elsevier.com/retrieve/pii/S0960897416300237>.